

Xin-Long Li^{1,2}, Jian-Hua Xu*^{1,2}, Wen-Ping Song^{1,2}, Shao-Qiang Han³, & Zhong-Hua Han^{1,2}

¹School of Aeronautics, Northwestern Polytechnical University, Xi'an 710071, China
²National Key Laboratory of Aircraft Configuration Design, Xi'an 710072, China
³Tianfu Engineering-oriented Numerical & Software Innovation Center,
College of Computer Science, Sichuan University, Chengdu, 610065, China

Abstract

As the helicopter hovers near the ground, the interactions among the rotor, the wake, and the ground complicate the flow field, altering the rotor's aerodynamic forces significantly. To investigate the influence of ground effect on the rotor aerodynamic characteristics, the flow around the rotor in hover is numerically simulated by using the in-house Computational Fluid Dynamics (CFD) codes with a structured dynamic overset grid system. A novel 5th-order WENO-K scheme based on nonlinear reconfiguration is employed for spatial discretization, effectively reducing the numerical dissipation and achieving high-accuracy capture of the tip vortices. In this study, the aerodynamic forces and flow fields of the S-76 rotor in ground effect and out ground effect are compared. The influence and mechanisms of ground effect on rotor aerodynamic characteristics are analyzed in detail. Results show that the ground effect causes a strong upwash flow in the inboard region of the blade and compresses the tip vortices, result in a significant increase in thrust at the blade root and a slight decrease in thrust at the blade tip, respectively.

Keywords: Helicopter rotor, Ground effect, High-order scheme, Unsteady flow

1. General Introduction

Hovering in ground effect (IGE) is a crucial flight mode for helicopters, including military and rescue helicopters. Due to the ground blockage, the tip vortices are compressed and expand outward, making the flow field more complex than that of out ground effect (OGE). This significantly alters the rotor air loads, affecting the aerodynamic performance and control stability of helicopters.

Many studies have investigated the influence of ground effect on rotor aerodynamic performance using experimental and theoretical analyses. In term of experiments, early experimental studies primarily focused on measuring rotor thrust and shaft power during hovering close to the ground [1]-[3]. These studies found that ground effect can effectively reduce shaft power and improve hovering efficiency. With the development of flow visualization technology, methods such as smoke flow [4], wide-field shadowgraph [5], and particle image velocimetry (PIV) [6] were utilized to measure the geometric shape of rotor tip vortices and analyze their evolution in ground effect. In term of theory, various aerodynamic models for ground effect were established in the early stages. Betz et al. [7] established a mirror method for modeling ground effect through momentum source theory, embodying the ground boundary conditions by using mirror sources. In addition, vortex theory [8], free wake theory [9], jet theory [10], and other methods were applied in the analysis of rotor aerodynamics in ground effect. However, these methods require extensive experimental data to obtain correction factors for the models. The applicability of theoretical methods is limited when solving the complex rotor flow fields and conducting detailed analyses of ground effect, making it challenging to apply them to various rotor configurations.

Therefore, to predict the flow around the rotor in ground effect more accurately, flow simulations based on first principles are essential. Kutz et al. [11] solved the flow of a single rotor in ground effect using the Reynolds Average Navier-Stokes (RANS) equation and conducted a detailed study of the

geometrical positions of tip vortices and rotor thrust coefficients. The calculated results agreed well with experimental values. Liand et al. [12] developed a CFD solver based on the unstructured embedded grid technique aiming to simulate the flow of a rotor in ground effect and accurately analyze the influence of ground effect on rotor aerodynamic characteristics. Hwang et al. [13] studied the aerodynamic performance of the S-76 rotor in hover for both OGE and IGE using a flow solver with an unstructured mixed mesh. The calculations were performed for three different blade configurations, including swept-tapered, rectangular, and swept-tapered-anhedral tip shapes.

In the present study, the CFD codes called PMNS3DR [14] with a structured dynamic overset grid system, developed by our research group, is utilized to simulate the viscous flow around the rotor in ground effect. To better resolve the flow characteristics and the wake structure, a novel high-order scheme [15] (WENO-K) proposed by our research group is utilized for spatial discretization. The flow field and aerodynamic characteristics of the S-76 rotor with swept-tapered tip shapes in hover are numerically investigated for both OGE and IGE.

2. Numerical Methodology

The PMNS3DR features a block-structured finite volume approach that utilizes a cell-centered grid metric. In the inertial coordinate system, the unsteady RANS equations in an integral form can be expressed as

$$\iiint_{\Omega} \frac{\partial \mathbf{W}}{\partial t} dV + \iint_{\partial \Omega} \overline{\overline{\mathbf{H}}} \bullet \mathbf{n} dS = \iint_{\partial \Omega} \overline{\overline{\mathbf{H}}_{v}} \bullet \mathbf{n} dS$$
 (1)

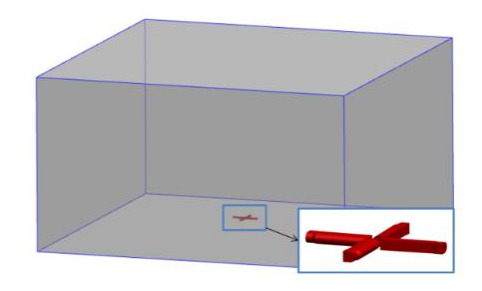
Where W is the vector of the conservative variables for mass, momentum, and energy equations. $\overline{\overline{H}}$ represents the Cartesian velocity components, and N is the outward normal vector on the control surface. $\overline{\overline{H}}_v$ denotes the viscosity flux term. For spatial discretization, the viscous fluxes are discretized using a second-order central scheme, and the inviscid fluxes are approximated by the Roe flux difference splitting scheme [15], which features good robustness and high resolution. The reconstruction of the interface variables from cell averages is the key for a finite volume method to achieve approximately high-order accuracy. The codes employ a novel 5th-order WENO-K scheme based on nonlinear reconfiguration for the reconstruction. A full implicit dual-time stepping method with LU-SGS sub-iteration is adopted for time discretization. Local time-stepping, implicit residual smoothing and multigrid method are applied to accelerate the convergence of sub-iterations.

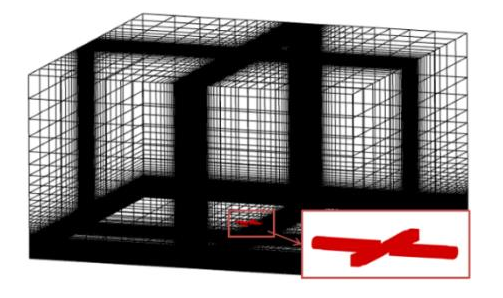
2.1 5th WENO-K Scheme For Spatial Discretization

Typical WENO schemes still suffer from excessive dissipation, which leads to severe dissipation of the rotor tip vortices and possible non-physical distortion. This paper introduces the 5th-order WENO-K scheme with Gauss-Kriging reconstruction and an adaptively optimized hyper-parameter to reconstruct left and right state values within the Roe Riemann solver for updating the inviscid fluxes. Through theoretical analysis and standard arithmetic validation [16], it is demonstrated that the WENO-K scheme has higher intermittent resolution and lower numerical dissipation than the traditional WENO scheme, while requiring only a small amount of additional computation time.

2.2 Structured Overset Grid System

High-quality grids and appropriate treatment for overset boundaries contribute to preserving the accuracy of flow simulation [17]. The structured overset grid system consists of a Cartesian background grid and several body-fitted blade grids, as shown in Figure 1(a) and (b). The background grid can be refined according to different flight states to capture the evolution of the rotor wake, with a minimum grid spacing of 0.07c in the cross-stream direction of the vortex core (where c is the chord length of the airfoil). Figure 2 shows the C-H rotor blade grid, where the first gird space normal the wall is strictly controlled according to y plus. After establishing the overset relationship between the rotor blade grid and the background grid, flow field information is interpolated. The code uses multiple layers of artificial boundaries to ensure that the 5th-order reconstruction accuracy of the hole boundary and the artificial external boundary is not reduced. Regarding the setting of boundary conditions, the bottom surface of the background grid is designated as a non-slip wall boundary to simulate the effect of the ground, as illustrated in Figure 3.

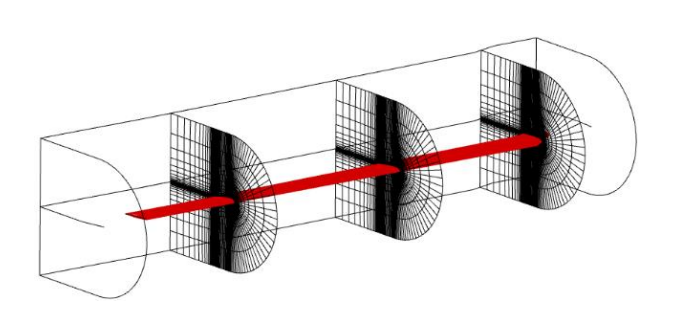


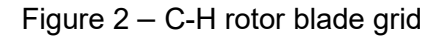


(a)Topology of background grid and blade grids

(b)Global view of background grid and blade grids

Figure 1 – Computational grid system





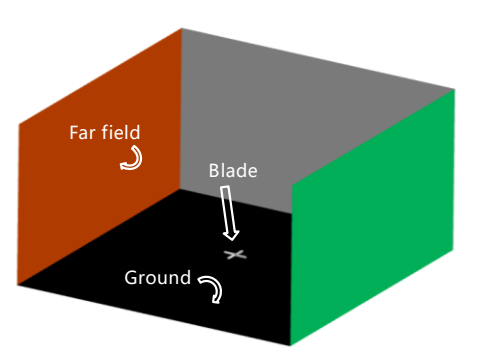


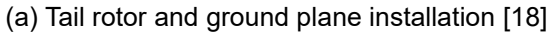
Figure 3 – Boundary condition

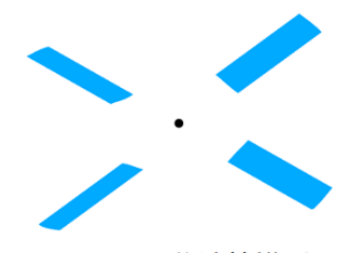
3. Results and Discussion

3.1 Validation

To verify the effectiveness of the code in simulating the flow around the rotor in ground effect, the Lynx tail rotor [18] hovering near the ground is selected as the validation case. The four-bladed Lynx tail rotor has a radius of 1.105m, with constant chord and untwisted blades, as shown in Figure 5. The sectional airfoil is NPL9615.







(b) Lynx tail rotor model

Figure 5 – Lynx tail rotor experiment and computational model

The Lynx tail rotor operates at the following conditions: tip Mach number $Ma_{tip}=0.56$, Reynolds number $Re=2.35\times10^6$, and total pitch angle 15°. The dynamic overset grid system consists of a background grid and four body-fitted blade grids. The size of the background grid is $241\times145\times241$ and the size of the rotor grid is $161\times41\times161$. The total grid number is about 12.87 million, the grid is shown in Figure 7. The height above ground is calculated at 4R, 2R, 1R, 0.52R, and 0.25R respectively, as shown in Figure 6.

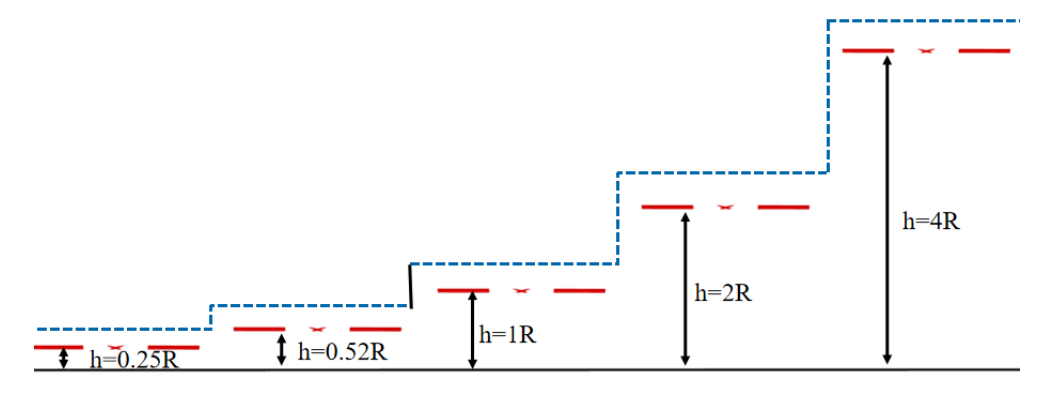


Figure 6 -Lynx tail rotor at different height above ground

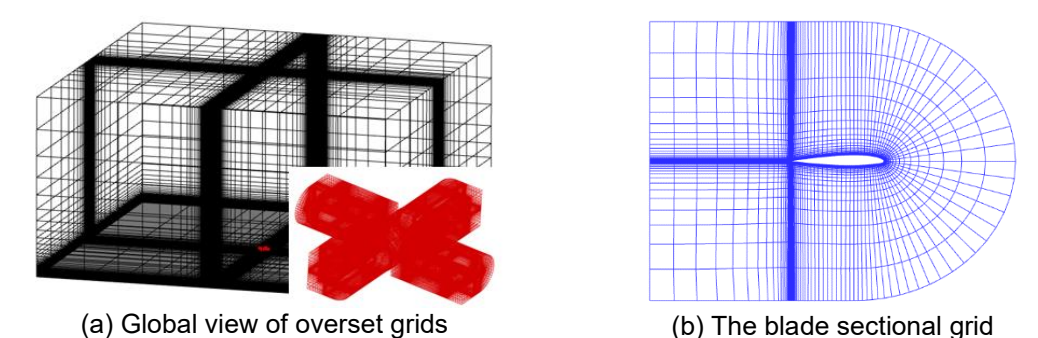


Figure 7 – Computational grid system of Lynx tail rotor

Figure 8 shows the thrust related to the thrust out ground effect at different non-dimensional rotor-ground distance (h/R), compared with experimental values and the Cheeseman empirical formula [19]. As shown in the figure, the thrust increasement decreases as the height above ground, and the calculated data are in good agreement with the experimental data. Figure 8 also shows that when the h/R is greater than 2, the ground has little influence on the rotor thrust, and the thrust related to the thrust out ground effect is close to 1, which is consistent with the actual physical situation. The increase in rotor thrust is an important feature when a helicopter is in hover near the ground.

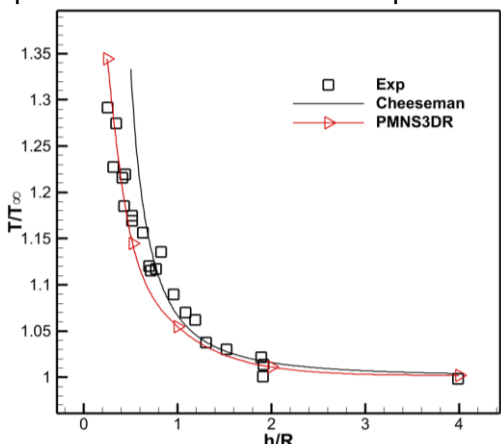


Figure 8 – Thrust prediction of Lynx tail rotor is in good agreement with the experimental data [18]

The tip vortices geometry position of the Lynx tail rotor at h/R=0.52 is shown in Figure 9, where "r" represents the radial position of the tip vortex and "y" represents the axial position of the tip vortex. This figure illustrates the significant influence of the ground on the tip vortex geometry. When the rotor is close to the ground, the axial distance of the tip vortex is greatly compressed, and the radial geometry of the tip vortex expands rapidly after a short contraction.

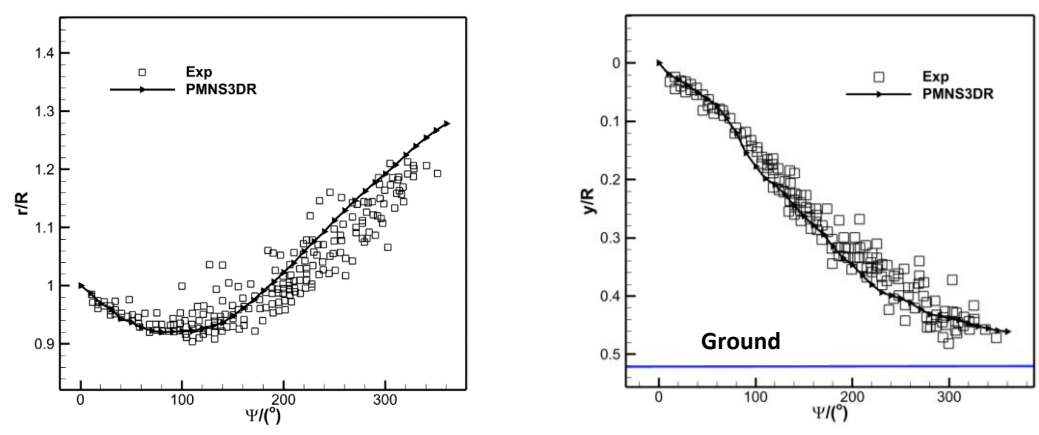


Figure 9 – The prediction of the Lynx tail rotor's tip vortex geometry of is in good agreement with the experimental data [18]

(h/R=0.52, left: radial position, right: vertical position)

3.2 S-76 Rotor Hover in Ground Effect

To investigate the ground effect on the helicopter rotor, the flow around the S-76 helicopter rotor [20] in hover is simulated in both IGE (h/R=0.75) and OGE. The model of the four-bladed S-76 rotor has a -10° linear twist and a solidity of 0.07043, as a 1/4.71 scale model. Each blade has a radius of 56.04 inches, a chord of 3.1296inches (aspect ratio 18.1), and uses the SC1013R8, SC1095 and SC1094 R8 airfoils. The tip section is swept by 35 degrees at 0.95R. The S-76 rotor geometrical shape is shown in Fig.10. The computational mode is shown in Figure 11.

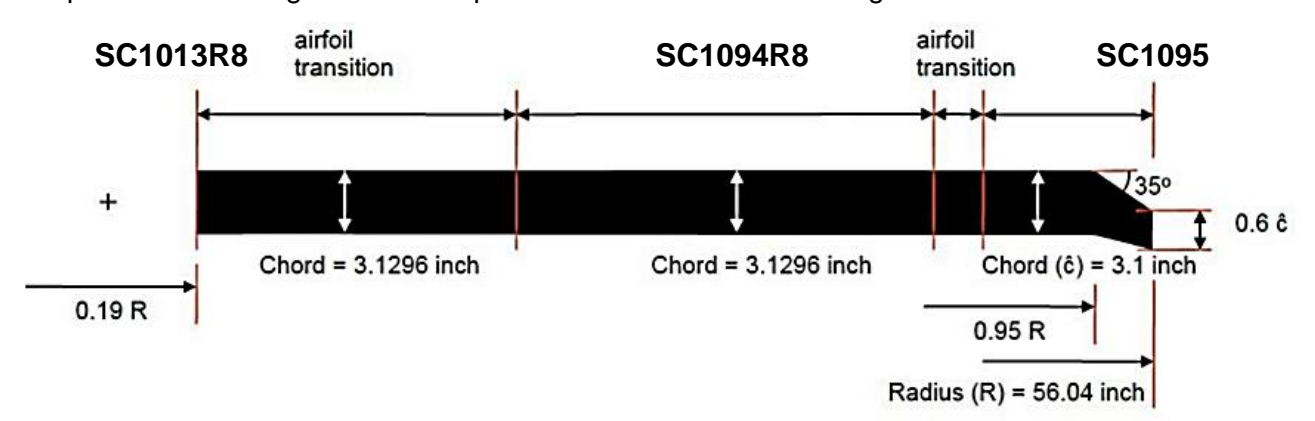


Figure 10 – The geometrical shape of the S-76 rotor blade [21]

Figure 12 shows the computational grid system of the S-76 rotor with a total number of 23.12 million grid cells. The bottom surface of the background grid is designated as a non-slip wall boundary except OGE condition. 10 revolutions of unsteady simulation are conducted, with each revolution of rotation is divided into 180 physical time steps ($\Delta \psi = 2^{\circ}$) with 25 sub-iterations for each time step. For both IGE and OGE, the tip Mach number (M_{tip}) is set as 0.65, and the pitch angle (θ) is 9 degrees.

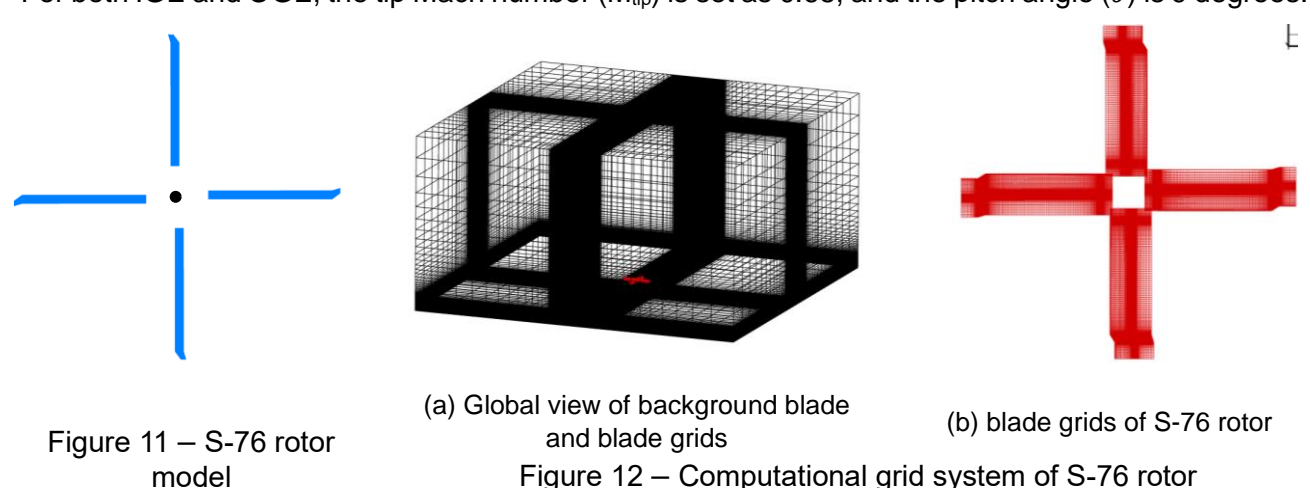


Figure 13 shows that the sectional pressure distribution is significantly affected by ground effect in the inboard region of the blade, and the pressure distribution area in ground effect is larger than that of out ground effect. At r/R=0.9, the pressure distribution between IGE and OGE is closer. Near the tip position with r/R=0.975, the pressure recovery in the case of OGE is slower. It is resulted by a flow separation on the upper surface of the airfoil as shown in Figure 14. This is different from the pressure distribution in the case of IGE. It indicates that ground effect slows down the separation at the blade tip of the S-76 rotor.

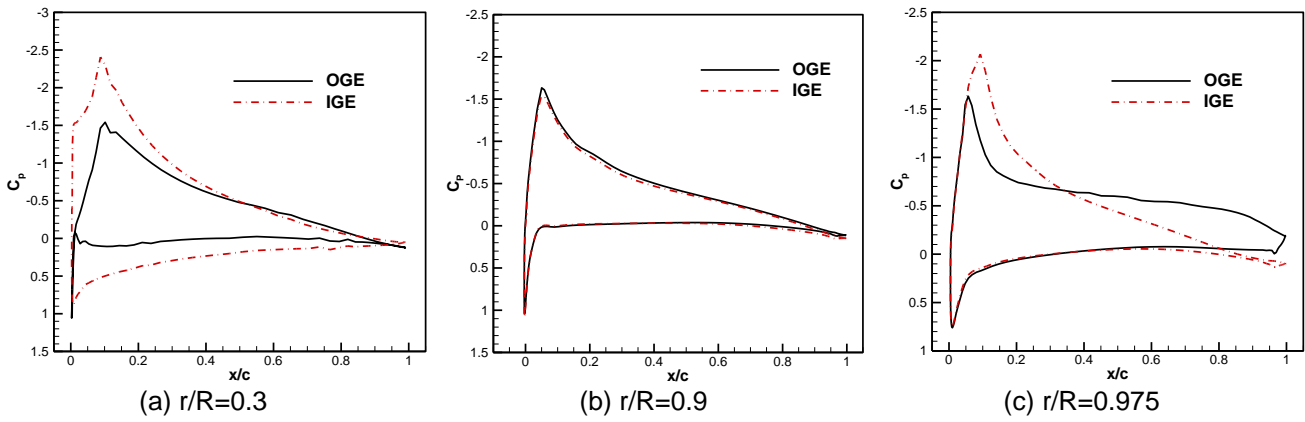


Figure 13 – The chordwise pressure distributions between IGE and OGE of the S-76 rotor at three spanwise stations

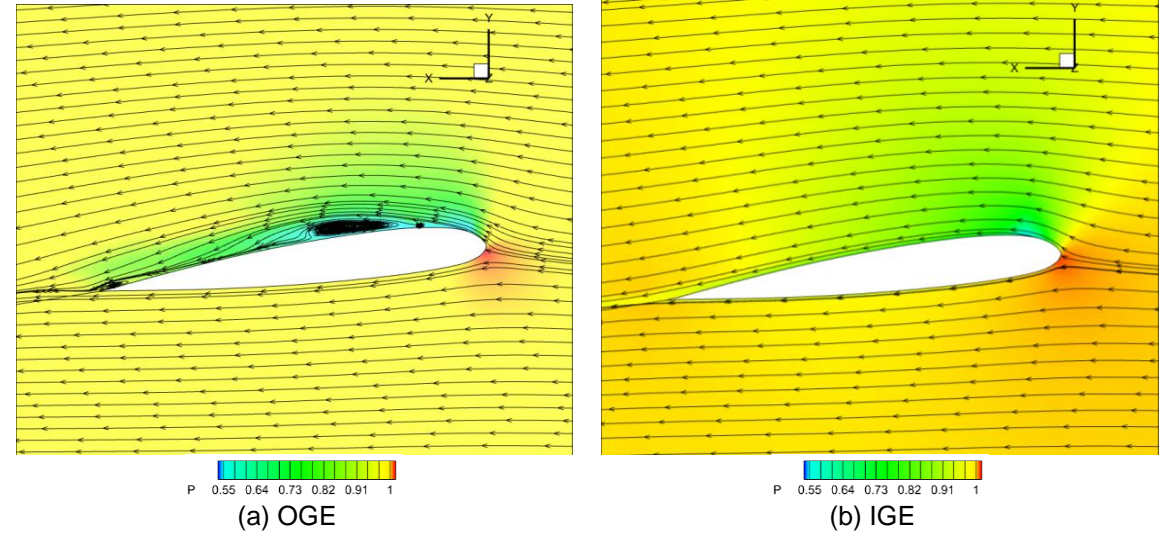


Figure 14 – The sectional pressure contours and streamline patterns for both OGE and IGE at r/R=0.975

As shown in Figure 15, there is a significant separation in the swept-tapered part of the blade, The comparison between OGE and IGE shows that ground effect weakens the separation and reduces the area of the separation region. In Figure 16, the sectional thrust coefficient in the inboard region of the blade is significantly increased by ground effect, but this effect gradually weakens along the spanwise direction. At the blade tip, influenced by the high induced velocity of the tip vortex, the sectional thrust coefficients decrease in both case of OGE and IGE, resulting in a "spoon-shaped" distribution. However, the sectional thrust coefficient in ground effect here is slightly lower than the case of OGE.

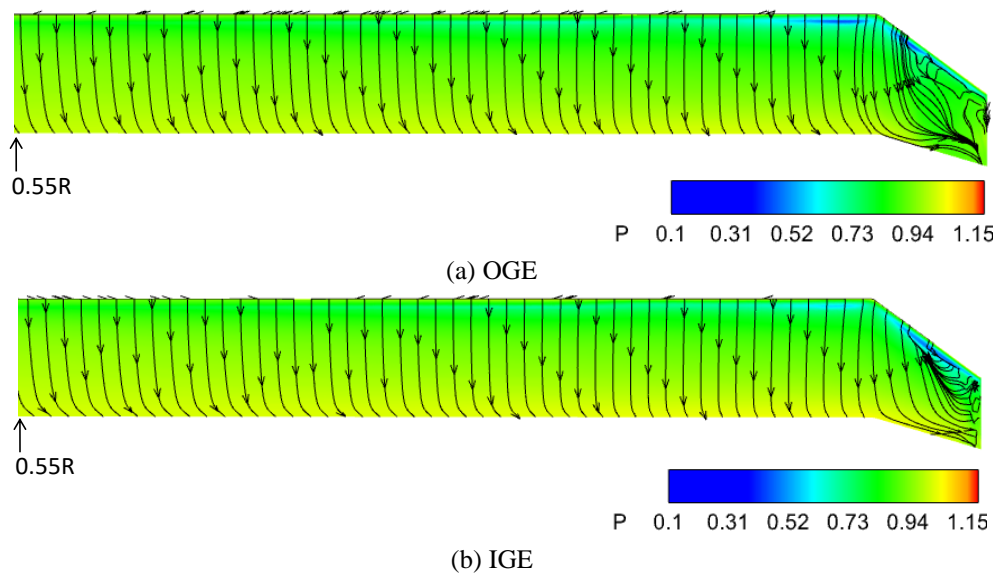


Figure 15 – The pressure contours and streamline patterns on the upper surface of the S-76 rotor between OGE and IGE

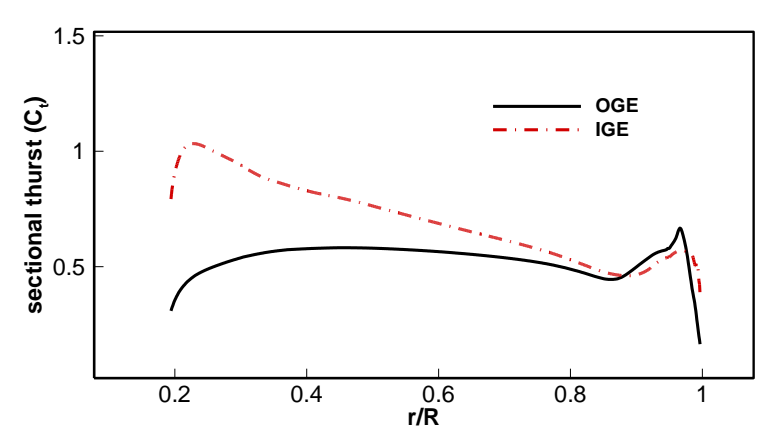


Figure 16 – The blade sectional thrust distributions along the spanwise direction between IGE and OGE

To further study the tip vortex and flow field affected by ground effect, the flow around the rotor is analyzed. Figure 17 shows that there is a strong upwash flow and circulation flow at the root of the blade under the blockage of the ground. This upwash flow increases the effective angle of attack in the inboard region of the blade, resulting in an increase in thrust. Additionally, the tip vortex generates high induced inflow at the tip region, and its downwash reduces the sectional thrust at the corresponding position, which is the main reason for the "spoon-shaped" sectional thrust distributions at the blade tip, as shown in Figure 18. In the case of IGE, the tip vortex of the rotor spreads outwards near the ground, and the streamlines become parallel to the ground.

In Figure 18, the wake structure of tip vortices and vortex sheets captured by 5th-order WENO-K scheme are very clear for both OGE and IGE. In the case of OGE, the tip vortices transport downward and gradually contract in the radius direction. However, in the case of IGE, the radial geometry of the tip vortex contracts for a short period, and then expands rapidly, eventually spreading outward along the ground plane. Near the ground, the tip vortices move downward along the shaft axis of rotor at a slower rate and the axial spacing of the tip vortices is smaller. The compressed tip vortices lead to a more significant downwash at the tip region, resulting in slightly lower sectional thrust, coefficients compared to that of OGE.

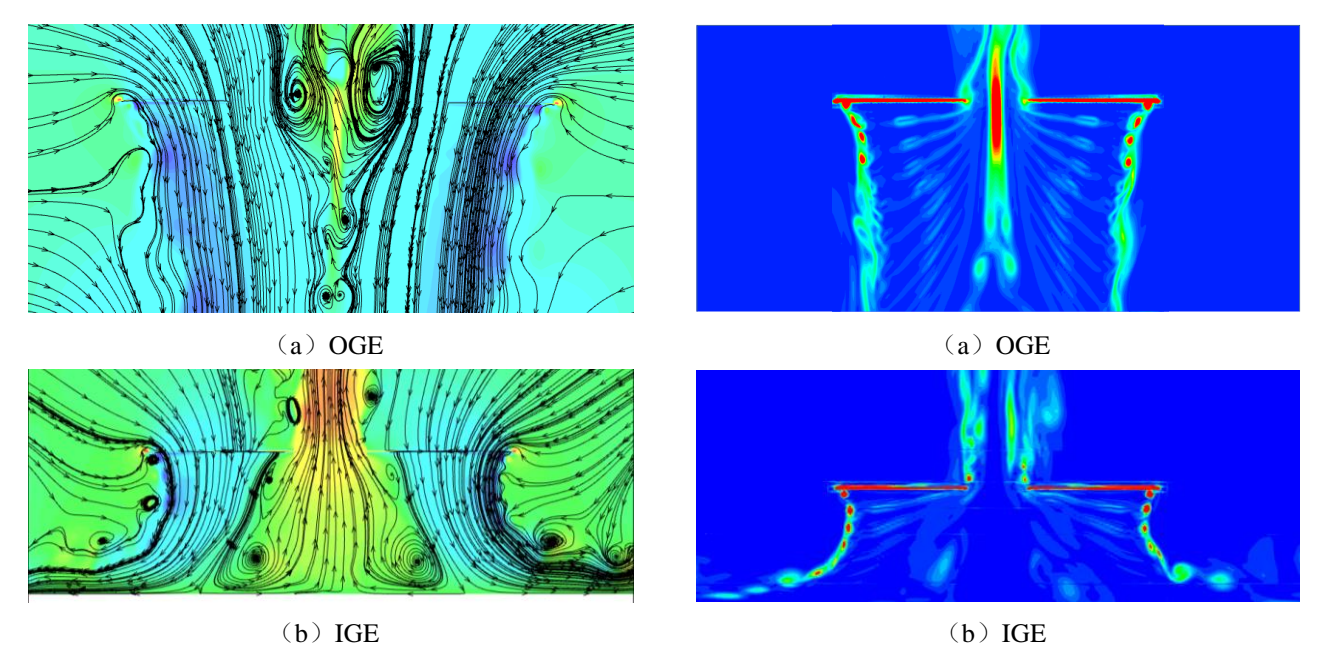


Figure 17 — The field streamlines and y-directional velocity contours between IGE and OGE at rotor vertical cutting plane

Figure 18 – The vorticity contours between IGE and OGE at the rotor vertical cutting plane.

4. Conclusion

In the present study, the unsteady flow around a rotor in hover state is numerically simulated using a novel 5th-orderWENO-K scheme. First, the flow of the Lynx tail rotor hovering near the ground is simulated to verify the method, and its thrust performance and the position of tip vortices show good agreement with the experimental data. Then, the flow of the S-76 rotor in both OGE and IGE is investigated. By comparing the rotor aerodynamic forces and flow field between OGE and IGE, the influence on aerodynamic characteristics and mechanisms of the rotor flow field in ground effect are concluded as follows:

- (1) The ground effect increases the rotor thrust coefficient. The sectional thrust increasement gradually decreases from the blade root to the tip, and the sectional thrust in the case of IGE is slightly lower than that of OGE at the blade tip.
- (2) Due to the blockage of the ground, there is a strong upwash flow and circulation flow at the root of the blade. This increases the blade effective angle of attack, leading to an increase in thrust.
- (3) In the case of IGE, the tip vortices expand rapidly after a brief contraction and move downward slowly near the ground. The compressed tip vortices cause a more significant downwash, resulting in a slight lower thrust at the blade tip and smaller the flow separation.

5. Acknowledgment

This research was sponsored by the Youth Innovation Team of Shaanxi Universities. The work was carried out at National Supercomputer Center in Xi'an, and the calculations were performed on Sugon.

6. Contact Author Email Address

Jian-Hua Xu *, xujh@nwpu.edu.cn.

7. Copyright Statement

The authors confirm that they, and/or their company or organization, hold copyright on all of the original material included in this paper. The authors also confirm that they have obtained permission, from the copyright holder of any third party material included in this paper, to publish it as part of their paper. The authors confirm that they give permission, or have obtained permission from the copyright holder of this paper, for the publication and distribution of this paper as part of the ICAS proceedings or as individual off-prints from the proceedings.

References

- [1] Hayden J S. The effect of the ground on helicopter hovering powering power require. *Proceeding of the 32nd American Helicopter Society Forum.* Washington, D C.; AHS,1976: 10-12.
- [2] Curtiss H C , Sun M, Putmanet W F, et al. Rotor aerodynamics in ground effect at low advance rations. Journal of the American Helicopter Society, 1984,29(1): 48-55.
- [3] Sheridan P F, Weisner W. Aerodynamics of helicopter flight near ground. *Proceedings of 33rd Annual Forum of American Helicopter Society*, 1997.
- [4] Curtiss H C, Sun M, Putnam W F, et al. Rotor aerodynamics in ground effect at low advance ratios. *Journal of the American Helicopter Society*, 1984, 29(1): 48-55.
- [5] Light J S, Tip vortex geometry of a hovering helicopter rotor in ground effect. *Journal of the American Helicopter Society*, 1993, 38(2): 34-42.
- [6] Ganesh B, Komerath N. Study of ground vortex structure of rotorcraft in ground effect at low advance ratios. 24th AIAA Applied Aerodynamic Conference, Reston, VA: AIAA,2006.
- [7] Betz A. The ground effect on lifting propellers: NACATM-836. Washington, D. C.: naca,1937.
- [8] He C J, Gao Z. A study of the rotor wake in nap of the earth. *Acta Aeronautica et Astronautica Sinica*, 1986,7(4): 325-331.
- [9] Duwaldt F A . Wakes of lifting propellers rotors in-ground-effect: CAL BB-1665-S-3. Washington, D.C. : CORNELL Aeronautical Lbortaory, 1966.
- [10] Preston J R, Troutman S, Keen E, et al. Rotor wash operational footprint modeling: RDMRAF-14-02. Middlesex: U.S. army Rdecom,2014.
- [11] Kutz B M, U. Kowarsch, M. Kebler, E. Kramer, Numerical investigation of helicopter rotors in ground effect. *Proc.* 30th AIAA Applied Aerodynamics Conference, 2012, AIAA-2012-2913.
- [12] Ye L, Zhao Q J, Xu G H. Numerical simulation on flow field of rotor in ground effect based on unstructured embedded grid method. *Acta Aeronautica et Astronautica Sinica*, 2009,30(5): 780-786.
- [13] Hwang J Y, Kwon O J. Assessment of s-76 rotor hover performance in ground effect using an unstructured mixed mesh method. *Aerosp Sci Technol* 2019: 84: 223-36.
- [14] Han S Q, Song W P, Han Z H. A novel high-order scheme for numerical simulation of wake flow over helicopter rotors in hover, *Chinese Journal of Aeronautics*, 2021
- [15] .Roe PL. Approximate Riemann solvers, parameter vectors, and difference schemes. *J Comput Phys* 1981;43(2):357–72.
- [16] Han S Q, Song W P, Han Z H. An Improved WENO Method based on Gauss-kriging Reconstruction with an Optimized Hyper-Parameter. *Journal of Computational Physics*, 2020:109742.
- [17] Han S Q, Song W P, Han Z H. A Computational study on blade-vortex interaction for coaxial rotors in hover using a novel high-order scheme. *ICAS*,2022.
- [18] LIGHT J S. Tip vortex geometry of a hovering helicopter rotor in ground effect. *Journal of the American Helicopter Society*, 1993, 38(2):34-42.
- [19] Cheeseman, I., and Bennett, W., The Effect of the Ground an a Helicopter Rotor in Forward Flight. *ARC R&M 3021*. Sep 1955.
- [20] N. Hariharan, R. Narducci, E. Reed, T.A. Egolf, Helicopter aerodynamic modeling of rotor with tip-shape variations. *AIAA standardized hover evaluations*, in: Proc. 54th Aerospace Sciences Meeting, 2016, AIAA 2016-0031.
- [21] Jain R K, Potsdam M A. Hover predictions on the Sikorsky S-76 rotor using Helios ,*AIAA Paper* 2014-0207.